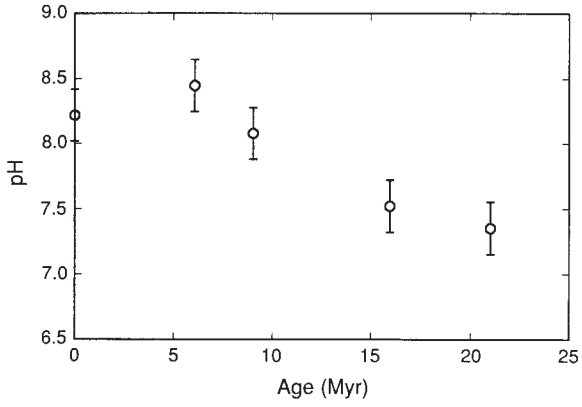

FIG. 3 Calculated pH values of surface sea water as a function of age. Values are based on the assumption that the B isotopic composition of sea water has been constant since 21 Myr ago and on the relationship between pH and isotopic fractionation established by Palmer *et al.*[16]. A best-fit line to their experimental isotope fractionation data between pH 6.70 and 8.45 is: fractionation (‰) = $-72.6 + 5.93 \times$pH with $R = 0.96$ and number of samples $n = 15$.

Calculated values are 8.2 ± 0.2 between the present and 7.5 Myr, decreasing to 7.5 ± 0.2 at 12.5 Myr and 7.4 ± 0.2 at 21 Myr ago (Fig. 3).

These pH variations imply changes in surface-water alkalinity and/or total inorganic carbon concentrations. In turn, surface-water variations in these properties can result from changes in whole-ocean average values and/or changes in their vertical distribution. Whole-ocean alkalinity and total inorganic carbon are functions of both continental and oceanic crust weathering and carbonate metamorphism rates, and their distribution within the ocean is driven by the imprint of biological processes on circulation[17]. Net productivity in surface waters and respiration in deeper waters results in a range of pH values from ~8.2 in typical surface waters to as low as 7.5 in parts of the deep ocean. Hence, the estimated seawater pH record implies considerable changes in global weathering and metamorphism and/or oceanic biogeochemical cycles, processes that also determine the atmospheric partial pressure of carbon dioxide[17,18].

Methods for reconstructing the CO_2 content of the ancient atmosphere, based on the carbon isotopic composition of marine organic matter and soil carbonates, have recently been developed. Using the isotopic composition of organic matter, Arthur *et al.*[3,4] have argued that the atmospheric partial pressure of CO_2 was 4.5 times the present value at 21 Myr ago, implying (as do our pH estimates[5]) that there have been changes in the surface-water carbon system. Soil isotopic data are consistent with higher CO_2 partial pressures 21 Myr ago, although within estimated uncertainties they do not rule out smaller variations[4].

If both CO_2 partial pressures and pH are known, all chemical species in the aqueous carbon system including alkalinity and total inorganic carbon can be calculated. For example, accepting the value of 4.5 times atmospheric CO_2 with a pH of 7.4 ± 0.2, then 21 Myr ago total carbon and alkalinity would have been $\sim 0.6 \pm 0.2$ times present-day values. Following the development of more detailed records, these properties could be used to constrain carbon-system geochemical models which have recently been the subject of intense debate[18–21]. □

Received 20 October 1992; accepted 23 March 1993.

1. Vengosh, A. *et al. Geochim. cosmochim. Acta* **55,** 1689–1696 (1991).
2. Hemming, N. G. & Hanson, G. N. *Geochim. cosmochim. Acta* **56,** 537–544 (1992).
3. Popp, B. N., Takigiku, R., Hayes, J. M., Louda, J. W. & Baker, E. W. *Am. J. Sci.* **289,** 436–454 (1989).
4. Cerling, T. *Am. J. Sci.* **291,** 377–400 (1991).
5. Arthur, M. *et al. Eos,* **259,** 166 (1991).
6. Kroenke, L. W. *et al. Proc. ODP Init. Rep.* **130,** 101–176 (Ocean Drilling Program, 1991).
7. Spivack, A. J., Palmer, M. R. & Edmond, J. M. *Geochim. cosmochim. Acta* **51,** 1939–1949 (1987).
8. Berner, R. A. *Early Diagenesis,* 241 (Princeton Univ. Press, Princeton, New Jersey, 1980).
9. McDuff, R. E. *Geochim. cosmochim. Acta* **45,** 1705–1714 (1981).
10. Delaney, M. L. *et al. Proc. ODP Init. Rep.* **130,** 549–552 (Ocean Drilling Program, 1991).
11. McDuff, R. E. & Gieskes, J. M. *Earth planet. Sci. Lett.* **33,** 1–10 (1976).
12. Spivack, A. J. & Edmond, J. M. *Geochim. cosmochim. Acta* **51,** 1033–1043 (1987).
13. You, C.-F., Spivack, A. J., Smith, H. J. & Gieskes, J. M. Geology (in the press).
14. Spivack, A. J. thesis, Massachusetts Institute of Technology/Woods Hole Oceanographic Institution (1986).
15. Kakihana, H. *et al. Bull. chem. Soc. Jpn* **50,** 158–163 (1977).
16. Palmer, M. R., Spivack, A. J. & Edmond, J. M. *Geochim. cosmochim. Acta* **51,** 2319–2323 (1987).
17. Broecker, W. S. & Peng, T.-H. *Tracers in the Sea* (Lamont-Doherty Geological Observatory, Palisades, New York, 1982).
18. Berner, R. A., Lasaga, A. C. & Garrels, R. M. *Am. J. Sci.* **283,** 641–683 (1983).
19. Raymo, M. E. & Ruddiman, W. F. *Nature* **359,** 117–122 (1992).
20. Caldeira, K., Arthur, M. A., Berner, R. A. & Lasaga, A. C. *Nature* **361,** 123 (1993).
21. L. M. Francois & Walker, J. C. G. *Am. J. Sci.* **292,** 81–135 (1992).
22. Manheim, F. T. & Sayles, F. L. *The Sea,* Vol. **5,** 527–568 (Wiley Interscience, New York, (1974).
23. Grinstead, R. R. & Snider, S. *Analyst* **92,** 532–533 (1967).

ACKNOWLEDGEMENTS. We thank the ODP and M. L. Delaney for providing samples.

Ultra-depleted primary melt included in an olivine from the Mid-Atlantic Ridge

A. V. Sobolev* & N. Shimizu†

* Vernadsky Institute of Geochemistry, Russian Academy of Sciences, Kosigin Str. 19, Moscow, 117975 Russia
† Department of Geology and Geophysics, Woods Hole Oceanographic Institution, Woods Hole, Massachusetts 02543, USA

MODELS of magma genesis at mid-ocean ridges[1], together with recent experimental data[2] and observations of trace element abundances in clinopyroxenes from abyssal peridotites[3], suggest that small-volume melt fractions can be efficiently extracted from the melting mantle. As shown in ref. 3, residues of this type of melting (fractional melting) display extremely low abundances of incompatible trace elements and extreme fractionation amongst them, especially at advanced stages of the process because of the compounded effects of differences in the partition coefficients. If this process operates beneath mid-ocean ridges, one would expect to sample melts that are correspondingly depleted and fractionated in trace elements. Indeed, the existence of very depleted melts in mid-ocean ridges was predicted previously[4–6] in order to explain the presence of magnesian pyroxene and calcic plagioclase in mid-ocean-ridge basalts. We report here the discovery of melt that has major and trace element characteristics consistent with these predictions[4–6], occurring as an inclusion in an olivine phenocryst in a typical mid-ocean-ridge basalt from the Mid-Atlantic Ridge. Although our preferred model for the origin of this 'ultra-depleted' melt is critical (continuous) melting, we cannot at this stage rule out other models. Our results underscore the importance of trapped melt inclusions as recorders of the processes involved in melting and melt extraction, and also as pointers to primary melt compositions.

The basalt sample in which the ultra-depleted melt (UDM) inclusion was found was dredged from the axial valley in an undisturbed segment of the Mid-Atlantic Ridge between the Doldrums and Vema fracture zones (9° N, 39.5° W). Details of dredging and of mineralogy and melt inclusions in minerals have been presented elsewhere[7]. In brief, the sample consists of ~20–30% phenocrysts of olivine (Fo_{90-87}), plagioclase (An_{86-80}), clinopyroxene (Mg# 89–87) and spinel (Cr# 38–47) in a matrix glass of slightly evolved composition (Table 1).

TABLE 1 Major element compositions of phases

	Glass*	Quench cpx	Fe-rich opx	Liquid†	UDM (initial composition)	Host olivine	Opx inclusion	Spinel inclusion	Matrix glass	Glass inclusions (initial composition)		Expt liquid‡
SiO_2	54.5	51.8	55.8	54.4	52.9	40.6	55.3	0.04	49.7	51.7	50.2	53.4
TiO_2	0.34	0.21	0.04	0.32	0.29	0.00	0.04	0.16	1.25	0.48	0.56	0.36
Al_2O_3	18.5	5.1	2.02	17.3	15.5	0.04	2.1	39.0	15.9	17.5	17.9	15.82
Fe_2O_3	nd	nd	nd	nd	0.7	nd	nd	5.6	nd	0.7	0.7	nd
FeO	6.5	5.2	6.58	6.45	6.4	9.8	6.1	8.8	9.2	5.9	6.3	6.74
MnO	0.09	0.08	0.13	0.09	0.08	0.15	0.13	0.13	0.20	0.09	0.11	nd
MgO	4.7	17.8	32.4	6.29	10.5	48.7	33.6	19.1	8.1	9.3	9.8	9.75
CaO	14.3	18.3	2.12	14.0	12.5	0.29	2.2	nd	11.8	12.2	12.3	12.77
Na_2O	1.35	0.15	0.06	1.25	1.12	0.00	0.06	nd	2.58	2.11	1.98	1.03
K_2O	0.00	0.00	0.00	0.00	0.00	0.00	0.00	nd	0.10	0.01	0.01	nd
Cr_2O_3	0.03	0.70	0.41	0.07	0.07	0.09	0.41	26.8	nd	nd	nd	0.21
Mg#	56.3	86.0	89.9	63.5	74.5	89.9	90.8	79.5	61.1	73.8	73.5	74.12

* Glass (UDM before corrections).
† Liquid after the first step of correction.
‡ Experimental liquid at 5 kbar and 1,250 °C (T-827) from ref. 19.
$Mg\# = 100 \times Mg/(Mg + Fe^{2+})$ in mole. Electron probe and analyses were made at the Vernadsky Institute, Moscow. Ferric iron in spinel was calculated on the basis of stoichiometry. Ferric iron in melts were calculated assuming wüstite–magnetite buffer (ref. 11). nd denotes not determined.

The UDM inclusion studied here was found in a 1-mm fragment of olivine phenocryst and has been described elsewhere[8]. The host olivine is uniform with ~Fo_{90}, and contains at least 10 melt inclusions of dimension ~100–10 μm and a few brown spinel inclusions. The glass inclusions generally have subspherical/ellipsoidal shapes with boundaries modified to a subplanar 'negative crystal'-like outline, which can be parallel to the extinction direction of the host. The distribution of the inclusions within the host crystal does not look like it is controlled by sealed cracks, which might be expected for inclusions of secondary origin[9]. Figure 1 shows that the UDM inclusion is ~60 × 40 μm in size and consists of clear glass (~80% in volume), a large euhedral crystal of orthopyroxene (opx) with very well developed facets, and feathery clinopyroxene (cpx) quench crystals grown on the opx. Table 1 summarizes chemical compositions of the phases. Other melt inclusions in the same olivine grain consist only of glass and shrinkage bubbles. Judging from the size of the opx crystal in the inclusion and the absence of opx in coexisting inclusions, we speculate that the opx was trapped in the host olivine together with the melt, rather than growing from the melt after entrapment. We consider that this inclusion is a primary melt inclusion rather than a melted polyphase crystalline inclusion. For instance, the opx within the inclusion is euhedral and unzoned (except for the quench rims) and does not show evidence for an unmelted precursor crystal. The host olivine is also unzoned and does not show evidence for resorption. The composition of the opx (Table 1) is consistent with being in equilibrium with the host olivine. It can be seen in Fig. 1, as has been observed previously[8] that the olivine wall surrounding the inclusion is richer in Fe than the host, indicating crystallization of olivine during quenching. Similar narrow, Fe-rich rims grown during quenching were observed on the opx. The cpx is evidently the result of quench crystallization within the inclusion.

The initial major element composition of the UDM was calculated in two steps. First, corrections for Fe-opx and quench cpx were made by adding 3.7 wt% of Fe-opx and 4.4 wt% of quench cpx to 91.9 wt% of the measured melt (Table 1). These proportions were derived previously[8]. Second, starting with the corrected melt composition, we corrected for post-entrapment growth of the host olivine by adding equilibrium olivine in 0.1 wt% increments to the melt and recalculating the equilibrium olivine composition, iterating until the equilibrium olivine composition became identical to the host olivine. The calculations used the formulation of ref. 10 with the oxidation state of iron corresponding to the wüstite–magnetite buffer[11]. As shown in Table 1, a 10 wt% correction was needed for deriving the initial UDM composition. For other inclusions in the same olivine host, only the latter correction was applied. Plagioclase, which could be expected to be in equilibrium with the glass, is not present in the inclusion, probably because of difficulty in nucleation or other kinetic factors.

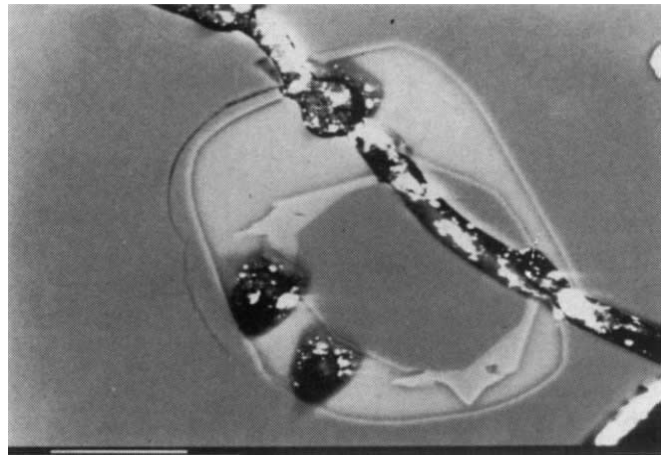

FIG. 1 Back-scattered electron image of the UDM inclusion in olivine. A fracture through the specimen has been enhanced by repeated polishing during the course of the study. Fe-rich olivine crystallized after entrapment can be seen as a thin brighter layer all the way along the wall of the inclusion. A large crystal with angular outline within the inclusion is opx, and Fe-rich rims can also be seen around it. Quench cpx occurs as irregular crystals attached to the sides of the opx. Bright speckles are remains of gold coating for ion probe analysis. Two ion probe pits are visible.

Trace elements in the UDM inclusion were analysed with a Cameca IMS 3f ion microprobe at Woods Hole Oceanographic Institution, using techniques described elsewhere[3,12]. In brief, energy-filtered secondary ion intensities of trace elements were converted to concentrations, using empirical relationships between intensity and concentration established from basalt glass standards. The accuracy and precision of the results are believed to be within ±10% for Ti, V, Cr, Sr, Y, Zr, Dy, Er and Yb, around ±20% for Ce, Nd, Sm and Eu, and ±40% for La. Two separate spots analysed in the UDM inclusion were identical within the analytical uncertainties. As the Ti content obtained by ion microprobe was close to that calculated in the initial melt composition, and in view of the analytical uncertainties, we did not make corrections for the post-entrapment crystallization.

The trace element chemistry of the UDM (Table 2) is unique in that all incompatible elements (except Ti and Na) are extremely depleted and that fractionation amongst incompatible elements is also extreme. For instance, Sr (1.3 p.p.m.) and Zr (2.9 p.p.m.) are in strong contrast to the values of 113 p.p.m. and 104 p.p.m., respectively, in average, normal mid-ocean-ridge basalt (NMORB)[13]; even very primitive MORB glasses (N.S. and A.V.S., unpublished results) have concentrations more than a factor of 15 higher than these. $[La/Sm]_N$, a measure of rare-earth element (REE) fractionation, is 0.04 in the UDM, as opposed to 0.65 in average NMORB[13] and 0.35 in primitive MORB (unpublished results). Furthermore, Ti/Zr is very high (594), compared with 93 in average NMORB[13] or 160 in primitive MORB (unpublished results), and adds to the uniqueness of the UDM. REE characteristics are illustrated in Fig. 2.

The major element composition of the UDM meets the petrological criteria for equilibrium with mantle minerals. First, the Mg# (75) is high enough for equilibration[4]. The formulations of Kinzler and Grove[14] indicate that the UDM can be in equilibrium with plagioclase lherzolite assemblage at 4.6 ± 1.6 kbar and 1,234 °C. Furthermore, the UDM composition is similar to a liquid (T-827) experimentally produced at 5 kbar, 1,250 °C from the Tinaquillo lherzolite[19] as shown in Table 1. This liquid is in equilibrium with a lherzolitic assemblage. The fact that the UDM composition is slightly more refractory than T-827 indicates that the UDM can be in equilibrium with a harzburgitic assemblage. We therefore suggest that the UDM is a primary mantle melt in equilibrium with a lherzolite/hazburgite residue. The petrological criteria support our contention that the UDM inclusion is a primary melt inclusion, rather than a melted polyphase crystalline inclusion.

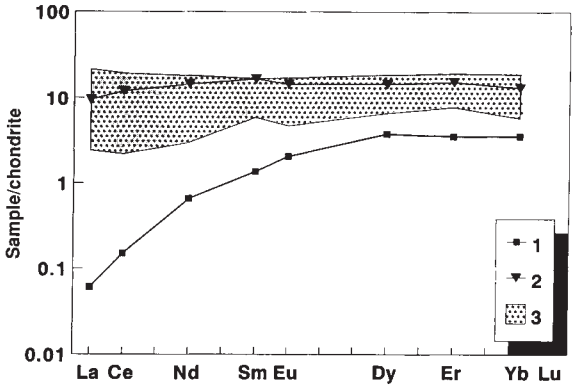

FIG. 2 Chondrite-normalized REE patterns of the UDM (■), the matrix glass (▲), and a range of primitive MORB glasses and glass inclusions (hatched area). Glass data are from unpublished results (A.V. and N.S.), and normalizing factors from ref. 18.

Two of the melt inclusions in the same olivine were analysed for major elements. They were subsequently ground away completely in the process of exposing the UDM inclusion and were not available for ion probe analysis. Their initial compositions (Table 1) have characteristics intermediate between the UDM and the matrix glass.

The geochemical characteristics of the UDM could be explained by a number of melting and melt extraction models. It is evident, however, that a simple single-stage batch melting process from a fertile mantle source cannot produce the required depletions in and fractionations amongst incompatible elements (for example, the ratios La/Sm and Ti/Zr).

One of the possible mechanisms is critical (continuous) melting, whereby small-degree melting is followed by melt extraction, with some melt retained in the residue; unlike fractional melting in which melt is completely extracted, the retained melt efficiently buffers highly incompatible elements from being fractionated too much. This type of melting process was first proposed by Dick[15] and developed later by Langmuir *et al.*[16] as continuous melting and by Maaloe[17] as critical melting. Our model assumes that mantle can retain only a certain amount of melt, and that melting proceeds in a closed system until this level is reached. Above the critical level, the system can lose any small amount of excess melt. It is also assumed that the critical amount of melt is always retained in the residue. The UDM can be satisfactorily modelled as an instantaneous melt fraction at 17 wt% melting of a depleted mantle with 2.2 wt% retained melt. Most of the UDM characteristics can also be produced by mixing melt fractions produced by fractional melting. A multi-stage melting model[5], in which the increments are fairly small and some melt is retained, can also adequately explain the UDM characteristics. In all possible mechanisms however, extraction of melt must follow each stage (or increment) of melting. Details of these melting models will be published elsewhere.

As mentioned earlier, the UDM could be in equilibrium with a lherzolite or possibly a harzburgite residue at pressures of ~5 kbar. This pressure is unusually low—pressures of ~10–20 kbar are usually discussed[20]. This suggests that the UDM could be the last fraction of melt produced in an ascending mantle column, representing the most advanced stage of critical (continuous) melting at the shallowest level. The matrix glass, on the other hand, could be derived from integration (polybaric mixing) of pre-existing melt fractions as suggested here. We further speculate that the chemical spectrum in primary MORB magmas is established among individual instantaneous melt fractions during critical (continuous) melting. Subsequent integration (mixing) to various degrees at decreasing depth would then produce a variety of parental MORB magmas. □

TABLE 2 Trace element concentrations

	UDM (p.p.m.)	Matrix glass (p.p.m.)
La	0.015	2.24
Ce	0.09	7.24
Sr	1.3	86.5
Nd	0.30	6.50
Zr	2.9	60.6
Sm	0.21	2.44
Eu	0.12	0.81
Ti	1,722	6,155
Dy	0.93	3.53
Er	0.62	2.43
Y	10.2	20.4
Yb	0.57	2.15

Received 11 December 1992; accepted 30 March 1993.

1. McKenzie, D. *Earth planet. Sci. Lett.* **72,** 149–157 (1985).
2. Riley, G. N. & Kohlstedt, D. L. *Earth planet. Sci. Lett.* **105,** 500–521 (1991).
3. Johnson, K. T., Dick, H. J. B. & Shimizu, *J. geophys. Res.* **95,** 2661–2678 (1990).
4. Green, D. H., Hibberson, W. O. & Jaques, A. L. in *The Earth: Its Origin, Structure and Evolution* (ed. McElhinny, M. W.) 265–290 (Academic, 1979).
5. Duncan, R. A. & Green, D. H. *Geology,* **8,** 22–26 (1980).
6. Duncan, R. A. & Green, D. H. *Contrib. Miner. Petrol.* **96,** 326–342 (1987).
7. Sobolev, A. V., Danyuchevskiy, L. V., Dimitriev, L. V. & Sushchevskaya, N. M. *Geochem. int.* **26,** 128–133 (1989).
8. Danyushevskiy, L. V., Sobolev, A. V. & Dimitriev, L. V. *Trans. USSR Acad. Sci. Earth Sci. Sec.* **292,** 102–105 (1988).
9. Roedder, E. *Rev. Mineral.* **12** (1984).
10. Ford, C. E., Russell, D. G., Craven, J. A. & Fisk, M. R. *J. Petrol.* **24,** 256–265 (1983).
11. Kilinc, A., Carmichael, I. S. E., Rivers, M. L. & Sack, R. J. *Contrib. Miner. Petrol.* **83,** 136–140 (1983).
12. Shimizu, N. & Hart, S. R. *A. Rev. Earth planet. Sci.* **10,** 483–526 (1982).
13. Hofmann, A. W. *Earth planet. Sci. Lett.* **90,** 297–314 (1988).
14. Kinzler, R. J. & Grove, T. L. *J. geophys. Res.* **97,** 6885–6906 (1992).
15. Dick, H. J. B. thesis, Yale Univ. (1976).
16. Langmuir, C. H., Bender, J. R., Bence, A. E., Hanson, G. N. & Taylor, S. R. *Earth planet. Sci. Lett.* **36,** 133–156 (1977).
17. Maaloe, S. *Geochim. cosmochim. Acta* **46,** 43–57 (1982).
18. Anders, E. & Grevesse, N. *Geochim. cosmochim. Acta* **53,** 197–214 (1989).

19. Falloon, T., Green, D. H., Hatton, C. J. & Harris, K. L. *J. Petrol* **29**, 1257–1282 (1988).
20. Falloon T. & Green, D. H. *J. Petrol. Spec. Lithosphere Issue*, 379–414 (1988).

ACKNOWLEDGEMENTS. We thank K. Ozawa and P. Kelemen for discussions on melting models, L. Danyushevskiy for providing us with unpublished data, H. Dick for organizing A.V.S.'s visit to WHOI, and K. Burrhus for maintaining the ion microprobe. This study was made possible by collaboration between Vernadsky Institute of Geochemistry and Woods Hole Oceanographic Institution, N.S. acknowledges support from the NSF.

Bioluminescent symbionts of flashlight fishes and deep-sea anglerfishes form unique lineages related to the genus *Vibrio*

Margo G. Haygood & Daniel L. Distel*

Marine Biology Research Division, 0202, Scripps Institution of Oceanography, University of California, San Diego, La Jolla, California 92093-0202, USA

* Present address: The Biological Laboratories, Harvard University, 16 Divinity Avenue, Cambridge, Massachusetts 02138, USA.

BIOLUMINESCENT symbioses range from facultative associations to highly adapted, apparently obligate ones[1]. The family Anomalopidae (flashlight fishes) encompasses five genera of tropical reef fishes that have large suborbital light organs[2]. The suborder Ceratioidei (deep-sea anglerfishes) contains 11 families. In nine of these, females have a bioluminescent lure[3,4] that contains bacterial symbionts[5]. In all other fish light-organ symbioses (occurring in 10 families in 5 orders[6]), the symbionts belong to three *Photobacterium* species[7]; nonsymbiotic luminous bacteria are *Vibrio* species[8]. The bacteria are extracellular and tightly packed in tubules that communicate with the exterior[7], releasing bacteria into the gut of the host or the surrounding sea water. The released bacteria are usually cultivable and can contribute to planktonic populations[9,10]. Although anomalopids release bacteria[9] and ceratioids have pores that would allow release, the fate of these bacteria is unknown and they cannot be cultured by standard isolation techniques. We report here phylogenetic analysis of 16S ribosomal RNA gene sequences from light organs that show that anomalopid and ceratioid symbionts are not known luminous bacteria, but are new groups related to *Vibrio* spp. They are characterized by host specificity, deep divergence between symbionts from different genera (anomalopids) or families (ceratioids) and, possibly, parallel divergence of hosts and symbionts.

In this study new 16S rRNA gene sequences were obtained (Table 1) and phylogenetic analysis was used to investigate the nature of the anomalopid and ceratioid symbionts. Inability to culture the bacteria could result from different mechanisms in the two groups. The symbionts may undergo irreversible physiological differentiation within the light organ, rendering them incapable of growth under culture conditions that might otherwise support growth of the undifferentiated cells. In this case they may be closely related to *Vibrio* or *Photobacterium* spp. Alternatively these symbionts could have genetically changed, losing adaptations that allow growth in nonsymbiotic environments and laboratory culture conditions, during a long period of obligate symbiosis in isolation from free-living populations. In this case one might expect deep divergence, and parallel divergence between symbionts and hosts. Our results support the latter hypothesis.

Polymerase chain reaction (PCR) amplification of 16S rRNA genes using universal eubacterial primers[11] followed by direct sequencing[12] allowed us to obtain data from light organs without cultivation of the bacteria. The anomalopid and ceratioid light organs contain pure cultures of symbionts; only one type of symbiont could be detected in a given light organ as shown by previous work[13–16]. Direct sequencing of 16S rRNA gene PCR products revealed only a single sequence. But low levels of a cosymbiont (<10% of the major symbiont population) could go undetected by these methods.

Parsimony analysis of the symbionts and representative γ-3 proteobacteria using PAUP shows that the anomalopid and ceratioid symbionts group with species in the genus *Vibrio* (Fig. 1). A similar result was obtained in a maximum likelihood analysis with fastDNAml (bootstrapped 100 times with input taxa jumbled, global rearrangement and a transition:transversion ratio of 2), with the exception that *V. cholerae* cannot be placed with confidence. The group containing the anomalopid and ceratioid symbionts and *V. harveyi* is supported at 92% in the maximum likelihood analysis. These results show that the anomalopid and ceratioid symbionts belong to species in the genus *Vibrio*, or new, allied genera analogous to *Photobacterium*. Thus the anomalopid and ceratioid symbionts appear to have arisen from the same common ancestor that was the source of the facultative *Photobacterium* light organ symbionts and other free-living luminous marine *Vibrio* spp., and the physiological differences that make them difficult to culture are probably due to evolution occurring after the establishment of symbiosis, rather than to a dramatically different phylogenetic origin.

The ceratioid and anomalopid symbionts do not belong to

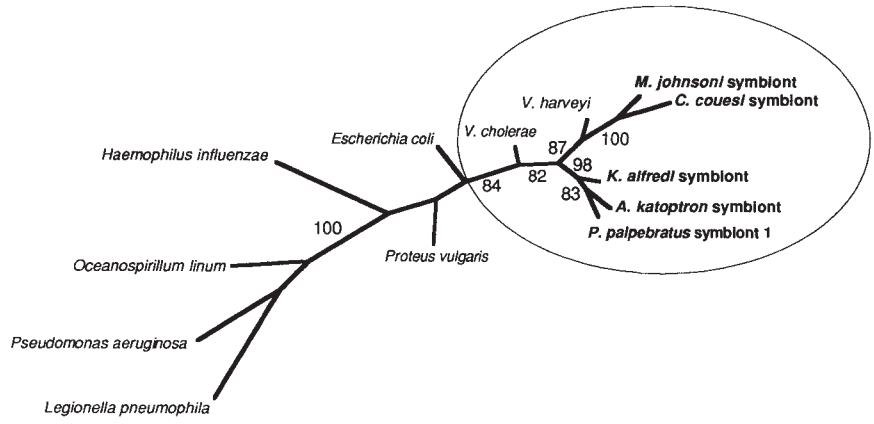

FIG. 1 Parsimony tree of γ-3 proteobacteria produced with PAUP with *Legionella pneumophila* (γ-2 proteobacteria) as the outgroup. The dataset used included 1,201 positions. The heuristic search algorithm was used with a transversion weight of 2. The dataset was bootstrapped 1,000 times with the starting tree constructed by random addition for each replication. Numbers beside branches are the per cent of bootstrap replications in which the group indicated appeared in the shortest tree (only groups supported at >80% are labelled).
METHODS. DNA was prepared as in refs 13 or 22. Table 1 contains sources for sequences. Collection data can be found in refs 15 and 16, with the exception that the *K. alfredi* sample was collected at Roatan, Honduras in 1990. Amplification and sequencing were according to refs 12 and 16. Sequence from each primer was read through the next priming site, so sequencing runs overlapped, except in the case of *P. palpebratus* 2, which was partially sequenced. Sequences were aligned to the *Escherichia coli* 16S rRNA secondary structure, checked for complementarity of helical regions and analysed with the Olsen phylogenetic analysis programs[23–25], PAUP[26], PHYLIP 3.41[27] and fastDNAml[28]. Indels and hypervariable regions that could not be reliably aligned were excluded from analysis.